Proceedings of the 7th European VLBI Network Symposium
Bachiller, R. Colomer, F., Desmurs, J.F., de Vicente, P. (eds.)
October 12th-15th 2004, Toledo, Spain

A Phase-reference Study of the CSS Radio Source 3C 138 at 15 GHz

L.-L. Shang[1,2], Z.-Q. Shen[1], X. Chen[1,2], and H.-B. Cai[1,2]

[1] Shanghai Astronomical Observatory, 80 Nandan Road, Shanghai 200030, P. R. China
[2] The Graduate School of Chinese Academy of Sciences, 19 Yuquan Road, Peking 100039, P. R. China

Abstract. We report on the phase-referenced VLBA mapping of a compact steep spectrum (CSS) source 3C 138 at 15 GHz. The single-dish measurements showed a total flux density of 1.63 Jy in 3C 138 at 15 GHz. Previous 5 GHz VLBI observations revealed that 3C 138 is a complicated lobe dominated source with mainly two emission regions: the central core and the eastern lobe which are separated by 400 mas at a position angle of 70°. Because of its being heavily resolved on longer baselines and the limited coherence time at high frequency, the SNR (signal-to-noise ratio) of 15 GHz VLBI observations is expected to be relatively low. So, as a part of our multi-frequency VLBI study of 3C 138 to probe its central activity, 15 GHz VLBA observation was carried out by using the phase referencing technique by fast switching between 3C 138 and a nearby bright compact quasar 0528+134. We will describe the use of a phase-referencing technique to map the source. A hybrid map from the detected visibilities of 3C 138 itself was also made. The maps of 3C 138 at 15 GHz exhibits 4 components in the central 10 mas region, consistent with the results from simultaneous observations made at 2.3, 5.0 and 8.6 GHz.

1. Introduction

The first VLBI phase-reference map with switching observation was released by Alef (1988). Self-calibration algorithms for the interferometer visibility have proven to work well in the high signal-to-noise ratio (SNR). When the SNR is low, however, the visibility phase will be determined ambiguously. Furthermore if it is below a flux limit imposed by relatively short coherence times no signal can be detected at all. To study the structure of very weak radio sources we should take advantage of phase-reference mapping (Alef 1989). This technique can hopefully work without the need for additional atmospheric or ionospheric calibration measurements. Currently phase-reference mapping has become a standard tool for imaging weak radio sources (Beasley & Conway 1995). While conventional imaging in VLBI provides information only about the relative position between different features in a given source, phase-referenced observations can provide precise positional information with respect to an external reference. Differential VLBI astrometry yields relative positions of radio sources with sub-milliarcsecond accuracy (Ros 2004). We will take advantage of this method to estimate the relative separation between the target and calibrator sources.

The radio source 3C 138 (=4C 16.12=J0521+166), located at RA $05^h21^m9^s.886$ and Dec $16°38'22''.052$, is identified as a quasar with $m_v = 18.84$ and $z = 0.759$ (Hewitt & Burbidge 1989). It is a compact, powerful quasar with a well-defined turn-over in the spectrum at about 100MHz and a steep high frequency spectrum of 0.65 ($S \propto \nu^{-\alpha}$), making it a prototype of the compact steep spectrum (CSS) sources (Fanti et al. 1990). The single-dish measurements from the 100-m telescope of the Max Planck Institute für Radioastronomie (MPIfR) shows that the total flux density is 1.63Jy at 15 GHz (Genzel et al. 1976). There are two emission regions at the previous 5 GHz map: the central core and the eastern lobe, which are separated by 400mas at a position angle of 70°, and there are several discrete emission components (Shen et al. 2001). The extended jet region emits most of the observed flux density (Cotton et al. 2003). At 15 GHz the resolution is three times higher than that at 5 GHz, so the diffuse lobes are resolved out and it enables us to study the core area in more detail.

2. Observations

We carried out fast-switching observation on 20th August 2001, using ten-25m VLBA antennas at 15.4 GHz. The observation was performed at multifrequency for 10 hours (10:00-20:00 UT), with 15 GHz observation interleaved of about 3 hours to ensure the comparable *uv* coverage. We used eight intermediate frequency (IF) channels with 8 MHz bandwidth per IF. The data was recorded at right-circular polarizations. The observation ran alternately between the target source 3C138 and the calibrators 0528+134 and J0539+1433. The observation included 2-minute scans on 0528+134 and J0539+1433, as well as periods of rapid switching between 3C 138 (scan lengths of 52s) and 0528+134 (scan lengths of 32s). Correlation was done at the VLBA correlator in Socorro, New Mexico (USA).

During the post-correlation data reduction, we first did a global fringe fitting to 3C 138 data directly and then made an image from the detected visibility data. The detailed process was given in section 3.1. Then we tried to make a phase-referenced map of the source 3C 138. We employed 0528+134 as the calibrator which is a compact strong γ-ray quasar. 0528+134 is located at RA $05^h30^m56^s.4167$ and Dec $13°31'55''.149$ and has a redshift $z = 2.06$. The separation of 3C 138 from 0528+134 on the sky is about $3°.91$. The compar-

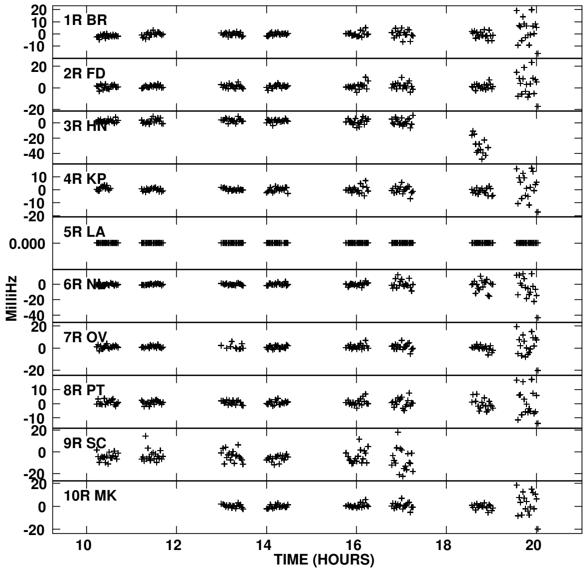

Fig. 1. Antenna rate solutions with respect to VLBA-LA for 0528+134 during a rapid switching period

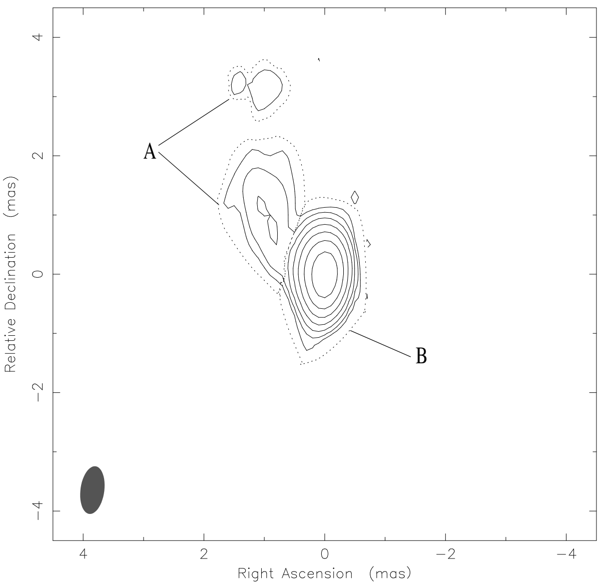

Fig. 2. VLBI map of 0528+134 with uniform weighting, contour levels are $(-1, 1, 2, 4, 8, 16, 32, 64) \times 13$ mJy beam^{-1}, peak 1.49 Jy/beam, CLEAN beam 0.812×0.395 *mas* at $-7.39°$ (indicated at the bottom of the left corner). The rms noise is 3.62 mJy beam^{-1}

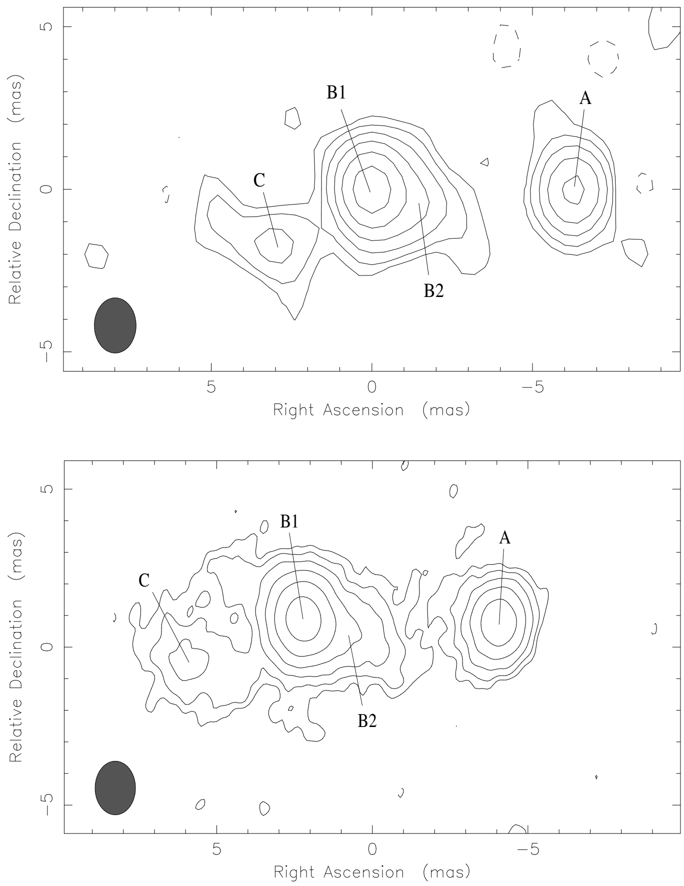

Fig. 3. VLBI hybrid map (upper panel) and VLBI phase-referenced map (lower panel) of 3C 138; uniform weighting. The restoring beam (shown at the bottom left corner of each map) is an elliptical Gaussian of $1.7 \times 1.3(mas)$ at 0°. Contours are 1.2 $mJy/beam \times (-1, 1, 2, 4, 8, 16, 32)$. Peak of hybrid map and phase-reference map is 62.0 mJy/beam and 55.1 mJy/beam respectively

ison between the results of two methods was given in section 4.

3. Data reduction

3.1. Hybrid mapping

We used the NRAO Astronomical Image Processing System (AIPS) for data reduction. We made a priori visibility amplitude calibration using system temperatures and gain curves from each antenna. We used the high SNR detections of 0528+134 on all baselines to calibrate the instrumental relative phases and delays between IF channels. VLBA-LA (Los Alamos at New Mexico) was used throughout as the reference station. During the initial fringe-fitting we set relatively wide search windows and SNR equal to 4 with a point source input model, and established residual delays and rates for all antennas and sources on all scans. This permitted us to use narrow search windows (delay 80nsec, 50mHz) for the next fringe search. We detected fringe on the baselines to six of ten VLBA stations (FD, KP, LA, NL, OV, PT). Finally we averaged all channels within each IF and transferred the data out of AIPS.

We used the Caltech imaging program DIFMAP (Shepherd et al. 1995) for mapping. We first averaged the visibility data to a 20-second grid with weights calculated from the scatter in the data. The data was then phase self-calibrated with a point source model, and several iterations of clean and phase-only self-calibration were carried out. We first began with uniform weighting; finally we switched to the natural weighting and performed several iterations of clean and self-calibration in phase again. For amplitude calibration, we only did an overall constant gain correction to each station. We used uniform weighting to show the map at maximum resolution in the upper panel of Fig.3. Having direct detection of the source 3C 138

Table 1. Circular gaussian model for hybrid mapping of 3C138

Component	S/(Jy)	r (mas)	θ (°)	a/(mas)
A	0.027	0	0	0.27
B2	0.024	4.93	94.3	1.62
B1	0.067	6.36	89.9	0.44
C	0.011	9.51	99.6	1.47

Table 2. Circular gaussian model for phase-reference mapping of 3C138

Component	S/(Jy)	r (mas)	θ (°)	a/(mas)
A	0.031	0	0	0.11
B2	0.021	4.88	94.2	1.47
B1	0.065	6.33	88.8	0.53
C	resolved			

Notes S: the flux density of each component; (r, θ): the distance and position angle of each component with respect to the component A; a: the radius of the circular component.

allows us to confirm the goodness of the phase-reference technique.

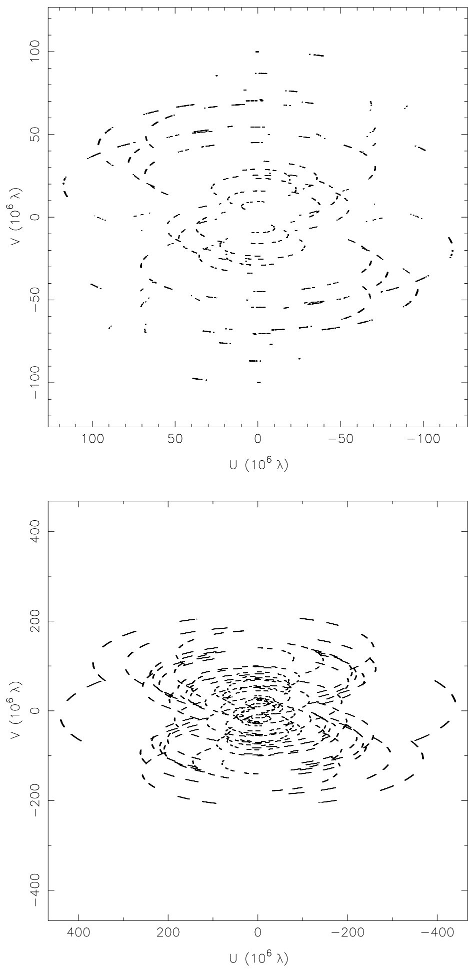

Fig. 4. The uv-coverage of the visibilities used in the hybrid mapping (upper panel) and the phase-reference mapping (lower panel)

3.2. Phase-reference mapping

We performed a phase-reference analysis within AIPS (e.g. Beasley & Conway 1995). Firstly, We made a priori visibility amplitude calibration and the instrumental phases calibration as we did in hybrid mapping. In order to remove structural phase effects from the reference source 0528+134 we mapped it with a high dynamic range (a peak-to-rms dynamic range of 400). Fig. 1 shows the antenna rate solutions from the reference source during a period of rapid switch and demonstrates that the solution can be easily reached between successive 32s scans. The map of calibrator 0528+134 is showed in Fig.2. Then the clean components of 0528+134 were fed back into the phase self-calibration process to produce the estimate of the antenna-based residuals, free from contamination by source structure. Finally, the antenna phase calibrations of 0528+134 were interpolated into the 3C 138 data. After this, the visibility data was transferred into Difmap. We followed the same step as we did in hybrid mapping except that we didn't employ a point source model. Fig.3 (lower panel) shows a phase-referenced map of 3C 138.

4. Analysis of the maps

A comparison between the hybrid map and the phase-referenced map of 3C 138 (Fig. 3) shows that both maps agree well. Our images of 3C 138 at 15 GHz exhibit 4 components in the central 10 mas region, Which is consistent with the results from simultaneous observations made at 2.3, 5.0 and 8.6 GHz (Shen er al. 2004). In general, we obtained a reliable map by phase-reference method. To yield a quantitative description, model fitting to both amplitudes and phases in the calibrated visibility data was applied. Table 1 presents the result of model-fitting to the hybrid map, which consists of four circular Gaussian components. Table 2 is the result of model-fitting to the phase-referenced map. The detailed comparison is shown as follows.

Firstly, We failed to fit the component C in the phase-reference map by one credible model. According to the uv-coverage plots (showed in Fig.4) of the visibility data resulted from the two calibration methods, we realize that more data were discarded in the hybrid mapping process, and the uv-coverage in phase-referenced map is larger and more uniform than hybrid map. The resolution in hybrid mapping is four times lower than that of phase-reference mapping. In addition, the component C is very diffuse. So we can't fit the component C in phase-reference mapping. There are some noise used in the phase-reference method, which will result in higher noise level in the phase-referenced map. The rms noise level in the map estimated from the visibility is 0.63 mJy/beam and 0.44 mJy/beam for hybrid map and phase-referenced map respectively. And the CLEAN beam size is 1.38×1.77 mas for hybrid map and 0.43×0.84 mas for phase-reference map. So the noise level in phase-reference map is higher than that in hybrid map. This is due to additional phase noise introduced by interpolating the reference phase and systematic errors caused by inaccuracies of the correlator models for the interfeometer geometry, propagation medium and earth rotation, etc.

Secondly, there is an offset of the peak-of-brightness distribution from the center of the phase-referenced map. The similar shift was measured in many other phase-referenced observations (Porcas & Rioja 2000; Alef 1988; Porcas & Rioja 2002). With respect to the peak-of-brightness of 0528+134, the peak-of-brightness of component A in the phase-reference map offsets by 2.1 ± 0.012 *mas* and 0.8 ± 0.016 *mas* in right ascension and declination respectively, where the quoted errors correspond solely to the uncertainty in determining the maximun of the brightness distribution in the image, based on the signal-to-noise ratio and the interferometric beam size, the error is $\sigma_{R.A.,Dec} = (1/2\pi) \times (1/SNR) \times (\lambda/D)$ (Lestrade at al. 1990). This reflects any error in the assumed relative separation in the correlator model. If the reference source has a true "point" structure and the separation between the target and calibrator sources is consistent with that adopted during correlation, the offset would be equal to zero.

Thirdly, there is a lower peak flux density in the phase-reference map (55.1 mJy/beam) compared with that in the hybrid map (62.0 mJy/beam), which contributes to the coherence loss. According to the phase-reference map the coherence loss in our system is about 11.1%. Generally speaking, our phase calibration using phase-reference method is successful. But there are also some anticipative errors which will cause the coherence loss in our system. The coherence of an interferometer is a measurement of the phase stability of the entire system (Rogers and Moran 1981). Although the residuals caused by instrument and propagation medium are assumed to be the same with respect to the target and calibrator sources and they can be effectively removed by phase-reference method, there are some facts influencing the effect of phase calibration in phase-reference method. First of all, because of the large separation between the target and calibrator sources (4° or so), the residuals caused by the propagation medium are not exactly the same, and the separation between the target and reference sources isn't the same as what was assumed in the correlator models. In addition, interpolating the reference phase can also introduce additional phase noise. Furthermore, the calibrator isn't exactly an point-source. In Fig.2, the integrated flux density inside the dotted circle A and B is 0.18Jy and 1.90Jy respectively, thus the integrated flux density of the non-point structure accounts for 8.6% of the total flux density of 0528+134. All of these factors will cause inaccurate phase calibration and results in coherence loss. The coherence is the ratio of the time-integrated fringe amplitude to the instantaneous fringe amplitude (Linfield et al. 1989). Coherence losses anywhere in the system will degrade the SNR and cause a lower peak flux density.

5. Conclusions

In general, we have achieved reliable result not only by hybrid mapping but also by phase-reference mapping. The result of both methods is consistent. In view of the higher resolution the phase-reference method gives a better result. The core area of 3C 138 is complicate and relatively weak and the separation between 3C 138 and 0528+134 is almost 4°, despite these difficulties we made a successful study of the core area of 3C 138. Our maps reveal there are four components in the core area of 3C 138 at 15 GHz.

We also estimated the peak-of-brightness of core in the phase-referenced map. The offset of the peak-of-brightness of core from the reference point of the correlator model is 2.1 ± 0.012 mas and 0.8 ± 0.016 mas in right ascension and declination, respectively.

References

Alef, W. 1988, in IAU Symposium 129, ed. M. J. Reid, & J. M. Moran (Dordrecht: Kluwer) 523
Alef, W. 1989. Very Long Baseline Interferometry Techniques and Applications, ed. M. Felli and R.E. Spencer 1989, 97.
Beasley, A. J., & Conway J. E. 1995, in ASP Conf. Ser. 82, Very Long Baseline Interferometry and the VLBA, ed. J. A. Zensus, P. J. Diamond, & P. J. Napier, 1995 327
Cotton, W. D., Dallacasa, D., Fanti, C., et al. 2003, A&A 406, 43
Fanti, C., Fanti, R., Parma, P., et al. 1989, A& A, 217,44
Genzel, R., Pauliny-Toth, I. I. K., Preuss, E., Witzel, A., 1976, AJ, 81, 1084
Hewitt, A., & Burbidge, G. 1988, ApJS, 69, 1
Kameno, S., Inoue, M., Matsumoto, K., et al. 1995, PASJ, 47, 711
Lestrade, J.-F., Rogers, A. E. E., Whitney, A. R., et al. 1990, AJ, 99, 1663
Linfield, R.P., Levy, G.S., Ulvestad, J.S., et al. 1989, ApJ 336, 1105
Rioja, M. J., & Porcas R. W. 2000, A&A, 355, 552
Rogers, A.E.E., and Moran, J.M. 1981, IEEE Trans., IM-30 (No. 4), 283
Ros, E. 2004, in ASP Conf. Ser., High Precision Differential Astrometry, preprint
Shen, Z.-Q., Jiang, D.R., Kameno, S., Chen, Y.J. 2001, A&A, 370, 65
Shen, Z.-Q., Cai, H.-B., Chen, X., et al. 2004, in preparation
Shepherd, M.C., Pearson, T. J., & Taylor, G.B. 1995, BAAS, 26, 987